Accepted Manuscript

Study on the effects of interfacial interaction on the rheological and thermal performance of silica nanoparticles reinforced epoxy nanocomposites

Qian Guo, Pengli Zhu, Gang Li, Junjie Wen, Tianyu Wang, Daoqiang (Daniel) Lu, Rong Sun, Chingping Wong

PII: S1359-8368(16)32297-1

DOI: 10.1016/j.compositesb.2016.10.081

Reference: JCOMB 4680

To appear in: *Composites Part B*

Received Date: 14 October 2016

Accepted Date: 30 October 2016

Please cite this article as: Guo Q, Zhu P, Li G, Wen J, Wang T, Lu D(D), Sun R, Wong C, Study on the effects of interfacial interaction on the rheological and thermal performance of silica nanoparticles reinforced epoxy nanocomposites, *Composites Part B* (2016), doi: 10.1016/j.compositesb.2016.10.081.

Graphical Abstract

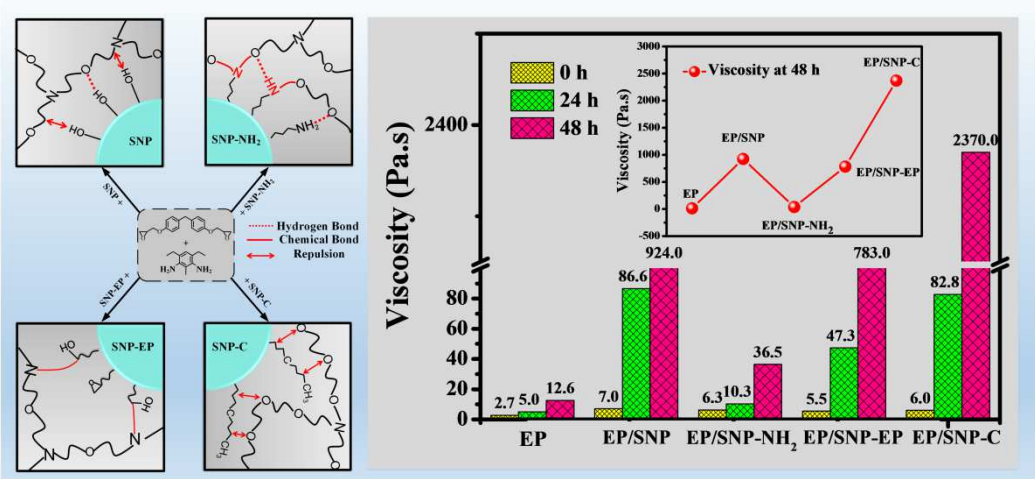

Attractive and repulsive interfacial interactions of the silica nanofillers with the amine-epoxy matrix were constructed and their great effects on the viscosity and viscosity stability of epoxy nanocomposites were reported.

Study on the effects of interfacial interaction on the rheological and thermal performance of silica nanoparticles reinforced epoxy nanocomposites

Qian Guo,[a,b] Pengli Zhu,[a,d,*] Gang Li,[a] Junjie Wen,[a] Tianyu Wang,[a] Daoqiang (Daniel) Lu,[a] Rong Sun, [a] and Chingping Wong [a,c,d]

[a]Shenzhen Institutes of Advanced Technology, Chinese Academy of Sciences, Shenzhen, China.

[b]Shenzhen College of Advanced Technology, University of Chinese Academy of Sciences, Shenzhen, China.

[c]School of Materials Science and Engineering, Georgia Institute of Technology, Atlanta, GA

30332, United States.

[d]Department of Electronics Engineering, The Chinese University of Hong Kong, Hong Kong, China.

*Corresponding Author: Tel.: +86-755-86392151; Fax: +86-755-86392299.

E-mail: pl.zhu@siat.ac.cn

Abstract

Three kinds of silica nanoparticles with different surface functional groups (amino groups, epoxide groups, and alkyl chain groups) were prepared and used as fillers in the amine-

cured epoxy resin systems to investigate the relationship between the interfacial interaction and the rheological and thermal properties of silica nanoparticles reinforced epoxy nanocomposites. It has been found that attractive interfacial interaction significantly contributed to reduce the viscosity and dramatically enhance the viscosity stability as well as reinforce the thermal stability of epoxy nanocomposites. While repulsive interfacial interaction had considerable negative effects on both of the viscosity and viscosity stability. Glass transition temperature of epoxy nanocomposites is closely related to the effects of the interfacial interaction on the curing process of bulk epoxy. This study may also shed lights on the choice of an optimum surface functional group for other inorganic fillers to improve the rheological properties and meanwhile keep good comprehensive thermal properties for epoxy nanocomposites.

Keywords: A. Polymer-matrix composites (PMCs); B. Interface/interphase; B. Rheological properties; B. Thermal properties

1. Introduction

Silica reinforced epoxy resins have been widely used as adhesives and encapsulants for electronic packaging in the microelectronics industry, because of their superior mechanical and electrical properties as well as the low cost and easy processibility [1,2]. The epoxy adhesives and encapsulants for electronic packaging are usually required to have a low viscosity for flowing and processing, and a high viscosity stability for a longer shelf life [3-5]. However, due to the premix of the epoxy resin and its curing agent, epoxy molecules cannot keep stable and begin to crosslink with each other under normal conditions, not only deteriorating the processibility, but also shortening the shelf life and the pot life of the

epoxy adhesives and encapsulants by dramatically increase the viscosity of the system [6,7]. Currently, the most commonly used method to address this problem is to use latent or microcapsule-type curing agent [4,8,9]. But the latent curing agent usually needs a higher curing temperature, while the microcapsule-type curing agent is normally very expensive [10].

Moreover, with the current miniaturization and multi-functionalization of the electronic devices, there is an ever increasing demand for the use of silica nanoparticles (SNPs) instead of the traditional micron-sized silica particles as reinforcing fillers in order to further improve the comprehensive performance of the epoxy resin and meet the new requirements for the modern electronics packaging technologies [11-14]. But, in comparison with the traditional micron-sized silica particles, SNPs usually cause a dramatic increase in viscosity as a result of their excessive surface energy and poor interfacial compatibility with the epoxy matrix [15,16]. This not only deteriorates the flowability and processibility of the nanocomposites, but also reduces the maximum filler loading of the nanocomposites and thus limits the improvement in its mechanical and thermal properties.

However, the large specific surface areas of the nanoparticles also provide an opportunity for tailoring the properties of their nanocomposites by creating a large amount of interfacial polymer layer with properties different from the bulk polymer, since the structure and property of the interfacial polymer layer has become one of the key factors in influencing the properties of the nanocomposites [17,18]. The structure and property of the interfacial polymer layer is closely related to the interfacial interaction between the inorganic filler and the polymer matrix [19]. If the surface chemistry of the inorganic filler is attractive to the polymer matrix, *i.e.* the surface functional groups of the filler could

either react with the polymer molecules or have good compatibility with them, the interface interactions can be strengthened. While, if the surface chemistry of the inorganic filler is repulsive to the polymer matrix, *i.e.* the surface functional groups of the filler could neither react with the polymer molecules nor have good compatibility with them, the interface interactions will be weakened [20]. Until now, a large body of scientific works has verified that the mechanical, thermal conductivity and dielectric properties of polymer nanocomposites can be adjusted by strengthen or weaken the interface interactions via surface engineering of inorganic fillers [21-27]. Therefore, all of the encouraging results inspired us to address the above mentioned problems by tailoring the interface interaction. Moreover, the effects of the interfacial interaction on the viscosity and viscosity stability of the SNPs reinforced epoxy nanocomposites has never been studied and reported so far.

Herein, in order to systematically investigate the relationship between the interface interaction and the rheological property of epoxy resin nanocomposites, in this study, SNPs with different surface functional groups (amino groups, epoxide groups, and alkyl chain groups) were prepared and used as fillers in the amine-cured epoxy resin systems. The SNPs surface modified with amino groups and epoxide groups were expected to form attractive interface interactions via chemical bonding due to their compatibility and chemical reactivity with the epoxy or amine hardener molecules. In contrast, the SNP surface modified with alkyl chain groups was used to form repulsive interface interaction because of the incompatibility and non-reactivity of the alkyl chain groups with both of the epoxy and amine hardener molecules. Further, the effects of the interfacial interaction on the rheological properties (shear response, viscosity, and viscosity stability) and thermal properties (storage modulus, glass transition temperature, thermal expansion behavior, and

thermal stability) of the SNPs reinforced epoxy nanocomposites were comparatively studied and discussed.

2. Experimental

2.1. Materials

SNPs used in this study were prepared by the classic Stöber method [28]. Their diameter was 60±10 nm. Before using, they were calcinated at 600 ^{o}C in a muffle furnace for 2 h. The silane coupling agents with the functional groups of amino group, epoxide group, and alkyl chain group, defined as Silane-NH_2, Silane-EP, and Silane-C, respectively, were purchased from Aladdin Industrial Inc and were used as modifiers for the surface functionalization of SNPs. Toluene and acetone used as solvents were purchased from Sinopharm Chemical Reagent Co., Ltd. For the formation of epoxy nanocomposites, diglycidyl ether of Bisphenol-F type epoxy resin (DGEBF, EPON 862, from Japan Epoxy Resin Co.) and diethyl toluene diamine hardener (DETDA, JER 113, from Japan Epoxy Resin Co.) were used.

2.2. Surface Modification of SNPs

The as-prepared SNPs with surface silanol groups were further functionalized by silane coupling agents as follows: Firstly, the as-prepared SNPs were well dispersed into 200 mL dry toluene via a ball-milling process. Next, the uniform dispersion was transferred into a 500 mL three-necked flask equipped with a mechanical stirrer, followed by adding a certain amount of silane coupling agent. Then the mixture was stirred at 90 ^{o}C for 48 h under reflux. Finally, the resulting surface functionalized SNPs were collected by centrifugation and washed with anhydrous ethanol. The final products were dried in a vacuum oven at 80 ^{o}C for 24 h before use. For the sake of convenience, the SNPs before and after surface

functionalization with amino groups, epoxide groups, and alkyl chain groups by silane coupling agents, are separately denoted as SNP, SNP-NH_2, SNP-EP, and SNP-C, respectively.

2.3. Preparation of Epoxy Nanocomposites

Epoxy nanocomposites filled with different types of SNPs were prepared by the following procedures. The fillers were firstly blended with epoxy and acetone, followed by being processed via a planetary ball mill at room temperature for 2 h. Then, the obtained homogenous dispersion was magnetically stirred at room temperature for 24 h in order to remove the acetone, and further degassed at 80 ^{o}C overnight in a vacuum oven to ensure the residual acetone was completely removed. Subsequently, the hardener was added to the above mentioned dispersion and mixed by a high-speed mixer under vacuum. Finally, the final bubble-free mixture was poured into molds and cured at 150 ^{o}C for 2 h and 200 ^{o}C for further 2 h, then cooled down to room temperature naturally to obtain the highly cross-linked epoxy nanocomposites. For comparison, the sample designated as EP for neat epoxy was also prepared in the same procedure. The cross-linking mechanism of the DGEBF cured with the DETDA hardener as well as the proposed mechanisms for the reaction between the epoxide and amino groups in the presence of the SNP-NH_2 and SNP-EP are given in Scheme 1.

2.4. Characterization

The Fourier-transform infrared (FT-IR) spectroscopy was used to characterize the surface chemistry of the SNPs. The absorption spectra were obtained on a VERTEX 70 Spectrometer in transmission mode. High-resolution X-ray Photoelectron Spectroscopy (XPS) analysis was performed on a VG scientific ESCALab 220I-XL using an Mg Kα X-

ray source. Thermo-gravimetric analysis (TGA) of the SNPs before and after surface modification as well as their epoxy nanocomposites was performed on a TA instrument Q-600 with a heating rate of 10 ^{o}C min^{-1} under an air flow rate of 100 mL min^{-1}. Fracture morphology observation of the composites was conducted on field-emission scanning electron microscope (FE-SEM, FEI Nova Nano SEM 450). The rheological behavior of the uncured liquid neat EP and its nanosuspensions was investigated with a rheometer (Anton Paar MCR 302). The measurements were performed at a steady flow mode with shear rate between 0.1 and 1000 s^{-1} at room temperature. The dynamic mechanical analysis (DMA) of the cured neat EP and its nanocomposites were carried out using a Q800 dynamic mechanical analyzer (DMA, TA Instruments, USA) in single-cantilever mode. Data were collected between 30 ^{o}C and 250 ^{o}C with a heating rate of 3 ^{o}C min^{-1} at a frequency of 1 Hz. The coefficient of thermal expansion (CTE) of the samples was conducted on a thermo-mechanical analyzer (TMA, NETZSCH Instruments, Model 402Fl). The data was determined between 30 ^{o}C and 250 ^{o}C at a heating rate of 3 ^{o}C min^{-1} after the second heating cycle. The chemical reactions of the silane coupling agents with the epoxy matrix were confirmed by the differential scanning calorimetry (DSC) (TA Instruments, Q2000) measurements under a nitrogen flow rate of 50 mL min^{-1} at a heating rate of 3 ^{o}C min^{-1} from 25 ^{o}C to 250 ^{o}C.

3. Results and discussion

3.1. Characterization of the Surface Chemistry of the SNPs

The morphology of the SNPs prepared by the classic Stöber method before and after calcination can be seen in Fig. S1 in the supplementary material. As shown in Fig. S1a, the as-prepared SNPs are monodisperse spherical particles with a size of about 60±10 nm.

After calcination, the morphology and the size of the SNPs did not show any obvious changes (see Fig. S1b). The surface of the SNPs prepared by the classic Stöber method is covered with richly silanol or hydroxyl groups, which makes them easy to aggregate with each other. As a result, in this work, for the surface modification of the SNP, it firstly went through a ball-milling process with toluene as solvent, in order to make the SNP fully disperse in the solvent and thus get a better effect of modification.

The surface chemistry of the SNPs before and after the surface modification was investigated firstly by FT-IR measurements within the mid infrared region (4000-500 cm^{-1}). In the FT-IR spectra of the SNP, SNP-NH_2, SNP-EP, and SNP-C (Fig. 1a), the strong absorption bands at 1110 cm^{-1} and 800 cm^{-1}, are assigned to the asymmetric stretching vibrations and the symmetric stretching vibrations of Si-O-Si, respectively. In addition, the broad absorption band at around 3400 cm^{-1} and the peak at 1637 cm^{-1} are attributed to the stretching vibration of surface hydroxyl groups and the bending vibration of surface absorbed water [29,30], respectively. In comparison with the spectrum of the as-prepared SNP, the new peaks at 2930 $cm^{-1}$and 2980 cm^{-1} in the spectra of SNP-NH_2, SNP-EP and SNP-C, which respectively correspond to the stretching vibrations of the $-CH_2$ and$-CH_3$ from the silane coupling agent molecules, proves that the amino groups, epoxide groups, and alkyl chain groups have been grafted on the particle surface, respectively.

The surface chemical compositions of the different types of the SNPs used in this work were further investigated by XPS. As shown in Fig. 1b, the wide scan spectra of all samples show the same peaks of O 1s, Si 2s and Si 2p as a result of the Si and O elements in silica molecules. In contrast with the spectrum of SNP, the new peak of N 1s at about 400 eV appears in the spectrum of SNP-NH_2. It can be further divided into two peaks at

399.7 eV for C–N and 401.6 eV for -NH_2 (Fig. 1c), which coincides well with the environment of the nitrogen atom in theSilane-NH_2 molecule, supporting the existence of amino groups from the Silane-NH_2 on the surface of the SNP-NH_2 [31]. The C 1s core-level spectra with peak-fitting curves of the SNP-EP and SNP-C are respectively shown in Fig. 1d and Fig. 1e. It can be seen that the C 1s spectrum of SNP-EP has binding energies at 284.8 eV for C−C species, at 287.6 eV for -CH(O)CH- species, at 286.2 eV for C-O species, and 284.1 eV for C-Si species. And the C 1s spectrum of SNP-C could be curve-fitted with C−C (284.8 eV), C-O (286.2 eV), and C-Si (284.0 eV) bonds. Both of the fitting results well coincide with the environment of carbon atoms in the Silane-EP molecule and Silane-C molecule, respectively, further indicating the success of the surface modification of the SNP with epoxide groups and alkyl chain groups.

TGA was used to estimate the weight ratio of the surface-grafted organic groups of surface-treated SNPs. The results are shown in Fig. 1f, and the related weight loss of samples at different stages as well as the calculated weight ratio of the surface-grafted silane groups (defined as W_{silane}) is summarized in Table S1. As can be seen from Fig. 1f, the SNP sample has an initial weight loss below 200 ^{o}C and a second weight loss after 565 ^{o}C, which attributes to the elimination of the physically absorbed water on the particle surface and the dehydration reaction between the surface or inner residual hydroxyl for the Stöber method prepared SiO_2, respectively [32]. While, the surface functionalized SNPs samples exhibit three decomposition stages in the investigated temperature range, *i.e.* lower than 200 ^{o}C, between 200-565 ^{o}C, and beyond 565 ^{o}C. It is clear that the surface functionalized samples exhibit a lower weight loss before 200 ^{o}C (2.07 wt%, 2.92 wt%, and 3.06 wt% for the SNP-NH_2, SNP-EP, and SNP-C, respectively, as shown in Table S1) as

compared with the SNP sample (4.25 wt%), which indicates the grafted silane molecules will take up some of the surface hydroxyl or prevent the absorption of water. In addition, in comparison with the SNPs sample, the additional weight loss between 200-565 ^{o}C of the SNP-NH_2, SNP-EP, and SNP-C, is caused by the decomposition of the surface silane functional groups. After calculation, the weight ratio of the surface-grafted silane groups is 3.69 wt%, 2.79 wt%, and 2.07 wt% for the SNP-NH_2, SNP-EP, and SNP-C, respectively, as collected and shown in Table S1. All of the differences in the TGA curves and the data in Table S1 between the SNP and the surfaced functionalized SNPs further support that the silane coupling agents have been grafted on the surface of the silica nanoparticles.

3.2. Rheological Properties of the Liquid Epoxy Based Nanosuspensions

Rheological properties, such as shear response, viscosity, and viscosity stability, play key roles in determining the processibility, flowability, and pot life of polymer matrix materials. The study of the shear response behaviors (*i.e.*, the viscosity changes with shear rate) of the neat EP and its nanosuspensions with 10 wt% SNP, SNP-NH_2, SNP-EP, and SNP-C under room temperature at 0 h, 24 h, and 48 h are respectively shown in Fig. 2a, b, and c. It can be seen that, at 0 h, the neat EP, exhibit Newtonian behavior (viscosity does not vary with shear rate) with a slight shear thinning behavior (viscosity decreases with shear rate) at high shear rate (over 464 1/s). The slight shear thinning behavior is due to the alignment of the epoxy molecules under the shear force [33]. After addition of the SNP, SNP-NH_2, SNP-EP, and SNP-C, the epoxy nanosuspensions of the EP/SNP, EP/SNP-EP, and EP/SNP-C are observed to have the similar shear response behavior as the neat EP, while the nanosuspension of EP/SNP-NH_2 shows the shear thinning characteristic from the beginning with its viscosity decreases significantly with the increase of the shear rate. The evident

shear thinning behavior of the EP/SNP-NH_2 at low shear rate (below 464 1/s) is attributed to the physical cross-linking caused by the hydrogen bonds of the epoxy molecules with the SNP-NH_2, which is easy to be destroyed under the external shear forces [34,35].

After 24 h and 48 h, the shear response of the neat EP still maintain a Newtonian characteristic, as shown in Fig. 2b and c. However, the nanosuspensions of the EP/SNP, EP/SNP-EP and EP/SNP-C exhibit the shear response of a Newtonian behavior at low shear rate and a strong shear thinning behavior at high shear rate, and the shear-thinning characteristic begins to start at lower shear rates with time. To be specific, at 24 h, it starts at 147 s^{-1} for all, while at 48 h it decreases to 10 s^{-1} for EP/SNP-C and 32 s^{-1} for EP/SNP and EP/SNP-EP. This can be attributed to the increased entanglement of the epoxy chains caused by the gradual chemical cross-linking with time [36]. For the nanosuspension of the EP/SNP-NH_2, the strong shear-thinning characteristic at low shear rate gradually disappear with time and develop into the Newtonian behavior after 48 h. The gradually weakened shear-thinning characteristic at low shear rate may be due to the chemical cross-linking of the epoxy molecules, which increases the resistance of the epoxy matrix to the external shear forces. In addition, the absence of the shear-thinning characteristic at high shear rate of the EP/SNP-NH_2 may be due to its lower cross-linking degree of the epoxy matrix as compared with the other nanosuspensions.

Fig. 2d shows the viscosity values at the shear rate of 1 s^{-1} of the neat EP and its nanosuspensions at 0 h, 24 h, and 48 h under room temperature, respectively. As shown in Fig. 2d, at 0 h, the viscosity values of the epoxy nanosuspensions are higher than that of the neat EP, indicating that the addition of silica nanoparticles will cause an increase in the viscosity of the neat EP. As for the epoxy nanosuspensions, at 0 h, the EP/SNP has the

highest viscosity value (7.0 Pa.s), followed it are EP/SNP-NH_2 (6.3 Pa.s), EP/SNP-C (6.0 Pa.s), and EP/SNP-EP (5.5 Pa.s) in sequence. The higher viscosity of the EP/SNP may be attributed to its poor dispersion and serious aggregation in the epoxy matrix [15,16,37]. While, the lower viscosity of the EP/SNP-EP is probably because of the good dispersion and compatibility of the SNP-EP in the epoxy matrix [37]. It is worth noting that the high viscosity value of the EP/SNP-NH_2 at the shear rate of 1 s^{-1} might be caused by the non-covalent interaction of the surface amino functional groups with the epoxy monomer, which leads to the EP/SNP-NH_2 exhibit gel-like behavior [34]. As shown in Fig. 2a, when the shear rate increases to 10 s^{-1}, its viscosity value becomes the lowest among the nanosuspensions, as a result of the destruction of the gel structure by the external shear forces. In order to further confirm the effects of the surface functional groups on the viscosity, the viscosity values of the EP nanosuspensions with 30 wt% filler loading at 0 h were also tested. As shown in Fig. S2 in the supplementary material, the EP/SNP-NH_2 and EP/SNP-EP has obviously lower viscosity, 34 Pa.s and 109 Pa.s, respectively, which are only 8.8% and 28.2% of the viscosity of the EP/SNP (386 Pa.s). While, the viscosity of EP/SNP-C is 27.2% (491 Pa.s) more than that of EP/SNP. Now, we can safely conclude that SNPs with surface amino groups and epoxy groups can decrease the viscosity of the EP nanosuspensions whereas the SNP-C has negative effect on the viscosity, especially at high filler loading level.

From Fig. 2d, it also can be clearly observed that the viscosity of the neat EP and its nanosuspensions increases as the increase of storage time at room temperature. As shown in Fig. 2d, the viscosity value of the neat EP is 2.7 Pa.s. After 24 h and 48 h, it increases by 0.9 times (5.0 Pa.s) and 3.7 times (12.6 Pa.s), respectively, as a result of the chemical cross-

linking between the epoxy molecules. After the incorporation of the SNP, the viscosity values exhibit a dramatic increase with time. As can be seen from Fig. 2d, the viscosity values of the nanosuspension of the EP/SNP dramatically increased by 11.4 times and 131.0 times after 24 h and 48 h (from 7.0 Pa.s to 86.6 Pa.s and 924.0 Pa.s), which are 1167% and 3441% more than those of the neat EP (0.9 times and 3.7 times), implying a great decrease in the viscosity stability. As compared with the EP/SNP, the viscosity values of the EP/SNP-NH_2, only increased by 0.6 times and 4.8 times (from 6.3 Pa.s to 10.3 Pa.s and 36.5 Pa.s), which are comparable to those of the neat EP (0.9 times and 3.7 times) and just 11.8% and 3.9% of those for the EP/SNP at 24 h and 48 h (86.6 Pa.s at 24 h and 924.0 Pa.s at 48 h), indicating a significant improvement in the viscosity stability of the epoxy nanosuspension. For the EP/SNP-EP, the viscosity values at 24 h (47.3 Pa.s) and 48 h (783.0 Pa.s) are 7.6 times and 141.4 times more than that of 0 h (5.5 Pa.s), which are 66.7% and 107.9% of those for the EP/SNP. While, as to the EP/SNP-C, the viscosity stability is further deteriorated when compared to the EP/SNP, since its viscosity values sharply increase by 12.8 times and 394 times (from 6.0 Pa.s to 82.8 Pa.s and 2370.0 Pa.s) after 24 h and 48 h, which are 112.3% and 300.8% of those for the EP/SNP. These data are also collected and shown in Table S2. The significant differences in the viscosity stability among the nanosuspensions, as can be directly observed from the inset in Fig. 2d, are presumably caused by the different interfacial interactions of the epoxy matrix (including epoxy monomers and hardener molecules) with the SNP, SNP-NH_2, SNP-EP, and SNP-C [38, 39]. As illustrated in Scheme 2, the interfacial interactions can be generally classified into two categories: repulsive and attractive. For the EP/SNP (Scheme 2a), the interfacial interaction is a repulsive one, due to the incompatibility of the surface polar hydroxyl

groups of the SNP with the epoxy segments. In comparison with the EP/SNP, the repulsive interfacial interaction of the EP/SNP-C is formed as a result of the strong repulsion between the surface non-polar long alkyl chain groups and the comparatively polar organic matrix (Scheme 2d), which will not only further impair the compatibility between the fillers and the epoxy matrix, but also could promote the epoxy cross-linking reactions by preventing the epoxy molecules physically absorbing on the surface of the fillers, thus resulting in the sharp decrease of the viscosity stability of the epoxy nanosuspension [40]. In contrast, as to the EP/SNP-NH_2 and the EP/SNP-EP, the chemical interactions of the SNP-NH_2 with the epoxy molecules and the SNP-EP with the diamine hardener [41,42], as shown in Scheme 1, lead to the formation of an attractive interfacial interaction (Scheme 2b and c). The above mentioned chemical reactions were certified by DSC study. As shown in Fig. S3, the endothermic peak and the exothermic peak in the DSC curves could demonstrate that there are some chemical reactions happening between the Silane-NH_2 and epoxy molecules as well as between the Silane-EP and DETDA molecules. These chemical interactions will inevitably produce an influence on the cross-linking process of the bulk epoxy molecules by altering the stoichiometric ratio of the diamine hardener molecules to the epoxy molecules, thus increasing the viscosity stability [43]. In addition, the physical interactions between the surface amino groups and the epoxy matrix such as hydrogen bonds and other Van der Waals' forces as discussed earlier may also passivate the cross-linking process of the bulk epoxy molecules, contributing to the significant enhancement on the viscosity stability. Therefore, from the discussion above, it can be concluded that the viscosity stability of the epoxy nanosuspensions can be controlled by tailoring the property of the interfacial interaction, and for improving the viscosity stability, the attractive interfacial

interaction formed with the fillers with surface amino functional groups is the optimum choice.

3.3. Dispersion and Interface Adhesion of SNPs in the Cured Epoxy Matrix

The dispersion state and the interface adhesion of the SNP, SNP-NH_2, SNP-EP, and SNP-C in the cured epoxy matrix were evaluated by SEM characterization on the fractured surface of their nanocomposites. As shown in Fig. 3a and b, it can be clearly observed that the SNP is prone to form large agglomerates in the epoxy matrix as a result of their excessive surface energy and the incompatibility between their polar surface silanol groups and the relatively non-polar epoxy matrix [44]. In comparison, after surface functionalization, the dispersion of SNP-NH_2 (Fig. 3c and d), SNP-EP (Fig. 3e and f), and SNP-C (Fig. 3g and h) is greatly improved, among which the SNP-EP has the best dispersion in the epoxy matrix. Although there are still agglomerates in the samples filled with the SNP-NH_2, SNP-EP and SNP-C, they are small in size and less in number as compared with the one filled with SNP. For the SNP-NH_2 and SNP-EP, the improved dispersion should be attributed to their decreased surface energy and their improved compatibility with the epoxy matrix after surface functionalization with amino and epoxide groups. While for the SNP-C, the improved dispersion is mainly due to the increased repulsion between the particles and the decreased surface energy by replacing the active surface hydroxyl groups with the inert alkyl chain groups [45,46]. Another important observation from Fig. 3 is the sharp contrast in the interface adhesion, which can be generally classified into two kinds: strong and weak. For SNP and SNP-C, they exhibit a clear contrast with their surrounding epoxy matrix and are easy to be distinguished. Especially the SNP-C is even exposed without being coated with any epoxy layer. All these indicate a weak interfacial interaction between them and the

organic matrix. In contrast, according to the Scheme 1b and c, for the SNP-NH_2 and SNP-EP, their surface modified amino or epoxide group may take part in the epoxy curing process, and will be coated by a thick layer of polymer which make them have relatively weaker contrast with their surrounding epoxy matrix, demonstrating a strong interfacial interaction and good compatibility between them and the epoxy matrix.

3.4 DMA Properties of the Cured Epoxy Based Nanocomposites

The dynamic mechanical properties of the cured neat EP and its nanocomposites filled with SNP, SNP-NH_2, SNP-EP, and SNP-C at 10 wt% loading were investigated by DMA, and the corresponding data are summarized in Table 1. The storage modulus (*E'*) depended on temperature is plotted in Fig. 4a. And their *E'* values at glassy and rubbery state are compared and summarized in Fig. 4b. As shown in Fig. 4a, at 40 ^{o}C, the *E'* value of the neat EP is 2369.0 MPa. Then it falls gradually as temperature increasing together with a sharp drop in the vicinity of the glass transition temperature (T_g), after which it finally decreases to 29.2 MPa at 180 ^{o}C. The sharp decrease of the *E'* can be explained by the whole segmental motions of the polymer chains as a result of the rise of temperature. The cured epoxy nanocomposites show the similar change behavior of *E'* with temperature as the cured neat EP, but their *E'* values are higher than that of the cured neat EP, as compared in Fig. 4b. For example, the *E'* values of the EP/SNP are 2693.5 MPa at glassy state (40 ^{o}C) and 37.8 MPa at rubbery state (180 ^{o}C), which are 13.7% and 29.5% higher than that of the neat EP, respectively. The increment in *E'* is due to the higher Young's modulus of the rigid silica fillers and their restriction on the friction and the mobility of the polymer chains [47]. However, for the epoxy nanocomposites, their *E'* values are pretty comparable regardless of the type of the interfacial interactions, indicating that the interfacial

interaction cannot cause noticeable effects on the *E'* of the epoxy nanocomposites at this 10 wt% filler loading level.

Tan δ is the ratio of loss modulus (*E''*) to storage modulus (*E'*). The tan δ curves of the cured neat EP and its nanocomposites as a function of temperature are shown in Fig. 4c. All of the curves exhibit a relaxation peak in the measured temperature range as a result of the movement of the epoxy segments with the rise of temperature. The peak temperature of the relaxation process is usually used to determine the glass transition temperature (T_g). The peak temperatures of the samples are given in Fig. 4d. It can be seen that the T_g of the cured neat EP occurs at 164.5 ^{o}C .When incorporated with 10 wt% SNP, it shifts to a lower temperature (160.6 ^{o}C). The decrease in T_g can be attributed to the poor compatibility and the serious agglomeration of the SNP in the epoxy matrix, which makes the epoxy segments move more easily by creating extra free volumes [41,48-50]. In comparison with the SNP, the SNP-NH_2 leads to a further reduction in T_g to 158.3 ^{o}C, whereas the SNP-EP and SNP-C causes a rise in T_g to 163.4 ^{o}C and 163.9 ^{o}C, respectively. As discussed earlier, the SNP-NH_2 and the SNP-EP have an effect on the cross-linking reaction of the bulk epoxy by altering the stoichiometric ratio of the diamine hardener molecules to the epoxy molecules, which may reduce the cross-linking density of the bulk epoxy and thus resulting in a decrease in T_g [51-53]. But, for the EP/SNP-EP, due to the better compatibility and dispersion of SNP-EP in the epoxy matrix, the SNP-EP may hinder the movement of the epoxy segments via the stronger interfacial interactions, leading to an increase of T_g [39]. Therefore, the rise of T_g of the EP/SNP-EP is the result of the above competing factors. As to the SNP-C, its enhancement on T_g should be attributed to its improvement on the cross-linking density of the bulk epoxy by decreasing the physically absorbed epoxy molecules

on the filler surface during the curing process as a result of the repellence between the longer alkyl chains and the epoxy molecules [54].

3.5. TMA Properties of the Cured Epoxy Based Nanocomposites

The thermal expansion behavior of the cured EP and its nanocomposites as a function of temperature was examined by TMA. Their dimension change curves are plotted in Fig. 5 and the related data is summarized in Table 1. As shown in Fig. 5, the slopes of the dimension change curves for all of the samples show a gradual change with the temperature, which reflects the glass transition from the glassy state to the rubbery state. T_g values of the samples determined from the intersection of the linear slopes at the glassy and the rubbery regions, are reported in Fig. 5. Although the T_g values determined by the TMA are slight lower than those measured by DMA, the change of the T_g values after the addition of SNP, SNP-NH_2, SNP-EP, and SNP-C reflected by TMA further confirms the previous results obtained from the DMA.

The CTE values, calculated from the slopes of the dimension change curves below and above T_g in the temperature regions of 40-80 ^oC and 180-220 ^oC, respectively, are listed in Fig. 5. The CTE values of the neat EP at glassy and rubbery states are 68.1 ppm $^oC^{-1}$ and 187.7 ppm $^oC^{-1}$, respectively. After the incorporation of 10 wt% SNP, they are respectively reduced by 8.5% and 7.8%. The reduction in the CTE is mainly due to the much lower CTE value of the rigid SNP filler and their confinements on the movement of the polymer chains [55,56]. Theoretically, the stronger interface interaction could lead to a further reduction in the CTE values [57,58]. However, the interface interaction between the filler and the epoxy matrix in our study does not cause noticeable impact on the CTE of the nanocomposities as expected, maybe due to the confined interfacial volume at this low filler loading (10 wt%).

3.6. Thermalgravimetric Analysis of the Cured Epoxy Based Nanocomposites

The effect of the interfacial interaction on the thermal stability of the cured epoxy nanocomposites was investigated by TGA under air atmosphere. Fig. 6 shows the decomposition curves of the cured neat EP and its nanocomposites filled with the SNP, SNP-NH_2, SNP-EP, and SNP-C at 10 wt% loading. The characteristic degradation temperatures are collected in Table 1. Both the neat EP and its nanocomposites have similar decomposition profiles and exhibit two degradation stages. The first decomposition weight loss (during 300-450 ^oC) arises from the breakdown of the epoxy network [59]. The further weight loss during 450-650 ^oC is assigned to the decomposition of benzene rings [60]. The characteristic degradation temperatures at 10%, 50%, and 70% weight loss are selected and used to evaluate the thermal stability. At 10% weight loss, there is no appreciable increase being observed in the thermal stability of the nanocomposites with respect to the neat EP (see Table 1), since the degradation at this time is mainly caused by the breakdown of the bulk epoxy network which accounts for the most part of the nanocomposites. However, as the decomposition continuing, the thermal stability of the nanocomposites is found to slightly increase, *i.e.*, at 50% weight loss, the decomposition temperature increases by about 10 ^oC as compared to the neat EP. This slight increment in the decomposition temperature is reasonably attributed to the physical barrier effect for the presence of silica nanoparticles, which might hinder the degradation reactions of the epoxy network around them. The differences in the thermal stability of the nanocomposites can be clearly observed in the second decomposition stage on the TGA curves in Fig. 6. The decomposition temperature at 70% weight loss of the epoxy filled with SNP-NH_2 and SNP-EP is respectively about 38 ^oC and 18 ^oC higher than that of SNP and SNP-C filled epoxy,

see Table 1. The enhanced thermal stability is presumably attributed to the strong covalent bonding at the interface between the SNP-NH_2 and epoxy molecules as well as between the SNP-EP and diamine hardener molecules, which might further impede the degradation reactions of the interfacial epoxy and diamine molecules [60,61].

4. Conclusion

The effects of the interfacial interactions on the rheological and the thermal properties of amine-cured epoxy resin system were studied and discussed by use of three kinds of surface tread SNPs (*i.e.* SNP-NH_2, SNP-EP, and SNP-C) and the as received SNP to form attractive and repulsive interfacial interactions with the epoxy matrix. The rheological behavior of the liquid epoxy nanosuspensions with shear rates was investigated at different time. The EP/SNP-NH_2 exhibited different shear response from the others due to the physical and chemical interactions between the SNP-NH_2 and the epoxy matrix. In comparison with the SNP, the SNP-NH_2 and SNP-EP contributed to a decrease in the viscosity and an increase in the viscosity stability, while the SNP-C caused an increase in the viscosity and a decrease in the viscosity stability, which means a better or worse flowability and processibility as well as a longer or shorter pot life and shelf life for the amine-epoxy nanocomposites. In particular, The SNP-NH_2 had the most efficient enhancement on the viscosity and viscosity stability. The SEM micrographs of the fractured surface of nanocomposites confirmed the strong interactions of the epoxy matrix with the SNP-NH_2 and the SNP-EP due to the chemical bonding between them, as well as the weak interactions of the epoxy matrix with the SNP-C and the as-received SNP as a result of the repulsion between them. The DMA and TMA results demonstrated that the surface amino groups would decrease T_g, while the surface epoxide groups and alkyl chain groups could

raise T_g as compared to the SNP. There were no noticeable changes among the storage modulus values and CTE values of the epoxy nanocomposites with different interfacial interactions at 10 wt% filler loading. The TGA results indicated that the cured EP/SNP-NH_2 and EP/SNP-EP exhibited an enhanced thermal stability in comparison with the EP/SNP and EP/SNP-C. In conclusion, for improving the comprehensive performance (*i.e*, the flowability, processibility, pot life, and the storage stability as well as the thermal properties) of the amine-cured epoxy nanocomposites via interfacial interaction, the SNP-NH_2 is the optimum choice. Moreover, this work also provides a reference and guidance for improving the same properties of other kinds of polymer composites with different inorganic fillers.

Appendix A. Supplementary material

The SEM images of the morphology of the SNPs prepared by the classic Stöber method (a) before and (b) after calcination at 600 ^{o}C for 2 h; Table of the TGA results of the different types of SNPs; the shear response behaviors of the neat EP and its nanosuspensions with 30 wt% SNP, SNP-NH_2, SNP-EP, and SNP-C and their viscosity values at the shear rate of 1 S^{-1} under room temperature at 0 h; DSC curves of the reactions between the Silane-NH_2 and EP molecules and between the Silane-EP and DETDA molecules can be found, in the online version, at http://dx.doi.org/10.1016/j.compositesa.

Author Contributions

The manuscript was written through contributions of all authors. All authors have given approval to the final version of the manuscript.

Qian Guo and Pengli Zhu contributed equally to this work.

Acknowledgment

This work was financially supported by the National Basic Research Program of China (973 Program, 2015CB057206), the National Natural Science Foundation of China (21571186), Guangdong Innovative Research Team Program (No.2011D052 and KYPT20121228160843692), “Guangdong TeZhi plan” Youth Talent of Science and Technology (2014TQ01C102), Shenzhen Basic Research Plan (JSGG20150512145714246 and JCYJ20140610152828685).

References

[1] Lee SM. In epoxy resins: chemistry and technology. New York: Marcel Dekker Inc 1988: 783.
[2] Sun YY, Zhang ZQ, Wong CP. Influence of interphase and moisture on the dielectric spectroscopy of epoxy/silica composites. Polymer 2005;45:2297-305.
[3] Rasiah IJ, Ho PS, Manoharan M, Ng CL, Chau M. Rheological analysis of an underfill material. IEEE/CPMT electronics packaging technology conference 1998: 354-58.
[4] Benson RC, Farrar D, Miragliotta JA. Polymer Adhesives and encapsulants for microelectronic applications. Johns Hopkins APL Technical Digest 2008;28:58-71.
[5] Wong CP, Luo SJ, Zhang ZQ. Flip the chip. Science 2000;290:2269-70.
[6] Wang LJ, Wong CP. Studies of latent catalyst systems for pot-life enhancement of underfills. Advanced Packaging Materials: Processes, Properties and Interfaces 1999. Proceedings. International Symposium on. IEEE 1999: 67-72.
[7] Tsuchida K, Bell JP. A new epoxy/episulfide resin system for electronic applications-2: pot life and prepreg storage life evaluation. J. Adhes. Sci. Technol. 2000;14:1515-26.
[8] Wong CP, Shi SH, Jefferson G. High performance no-flow underfills for low-cost flip-chip applications: material characterization. Components, Packaging, and Manufacturing Technology, Part A, IEEE Transactions on 1998;21:450-8.
[9] Zhang ZQ, Shi SH, Wong CP. Development of no-flow underfill materials for lead-free solder bumped flip-chip applications. Components and Packaging Technologies, IEEE Transactions on 2001;24:59-66.
[10] Liu XD, Zhao CH, Sudo A, Endo T. Storage stability and curing behavior of epoxy-dicyandiamide systems with carbonyldiimidazole-Cu (II) complexes as the accelerator. J. Polym. Sci. Pol. Chem 2013;51:3470-6.
[11] Lu D, Wong CP. Materials for advanced packaging. Springer: New York 2009.
[12] Zhang ZQ, Wong CP. Recent Advances in flip-chip underfill: materials, process, and reliability. Advanced Packaging, IEEE Transactions on 2004;27:515-24.
[13] Wan JW, Zhang WJ, Bergstrom DJ. Recent advances in modeling the underfill process in flip-chip packaging. Microelectron. J. 2007;38:67-75.
[14] Sun YY, Zhang ZQ, Wong CP. Study on mono-dispersed nano-size silica by surface modification for underfill applications. J. Colloid Interface Sci. 2005;292:436-44.
[15] Sprenger, S. Epoxy Resin composites with surface-modified silicon dioxide

nanoparticles: A review. J. Appl. Polym. Sci 2013;130:1421-8.
[16] Guo Q, Zhu PL, Li G, Huang L, Zhang Y, Lu DQ, et.al. One-Pot Synthesis of bimodal silica nanospheres and their effects on the rheological and thermal–mechanical properties of silica–epoxy composites. RSC Adv. 2015;5:50073-81.
[17] Schadler LS, Kumar SK, Benicewicz BC, Sarah LL, Harton SE. Designed interfaces in polymer nanocomposites: A fundamental viewpoint. MRS Bull. 2007;32:335-40.
[18] Caseri W. Nanocomposites of polymers and inorganic particles: Preparation, structure and properties. Mater. Sci. Technol. 2006;22:807-17.
[19] Ciprari D, Jacob K, Tannenbaum R. Characterization of polymer nanocomposite interphase and its impact on mechanical properties. Macromolecules 2006;39:6565-73.
[20] Hanemann T, Szabó DV. Polymer-nanoparticle composites: From synthesis to modern applications. Materials 2010;3:3468-517.
[21] Siddabattuni S, Schuman TP, Dogan F. Dielectric properties of polymer-particle nanocomposites influenced by electronic nature of filler surfaces. ACS Appl. Mater. Interfaces 2013;5:1917-27.
[22] Shu S, Husain S, Koros WJ. A general strategy for adhesion enhancement in polymeric composites by formation of nanostructured particle surfaces. J. Phys. Chem. C 2007;111:652-7.
[23] Jiang D, Xing L, Liu L, Yan X, Guo J, Zhang X, et.al. Interfacially reinforced unsaturated polyester composites by chemically grafting different functional POSS onto carbon fibers. J. Mater. Chem. A 2014;2:18293-303.
[24] Huang XY, Jiang PK. Core-shell structured high-k polymer nanocomposites for energy storage and dielectric applications. Adv. Mater. 2015;27:546-54.
[25] Huang XY, Zhi CY, Jiang PK, Golberg, D, Bando, Y, Tanaka, T. Polyhedral oligosilsesquioxane-modified boron nitride nanotube based epoxy nanocomposites: An ideal dielectric material with high thermal conductivity. Adv. Funct. Mater. 2013;23:1824-31.
[26] Zhang Y, Han H, Wang N, Zhang PT, Fu YF, Murugesan, M, et.al. Improved heat spreading performance of functionalized graphene in microelectronic device application. Adv. Funct. Mater. 2015;25:4430-35.
[27] Huang XY, Iizuka T, Jiang PK, Ohki Y, Tanaka T. Role of interface on the thermal conductivity of highly filled dielectric epoxy/AlN composites. J. Phys. Chem. C 2012;116:13629-39.
[28] Stöber W, Fink A, Bohn E. Controlled growth of monodisperse silica spheres in the micron size range. J. Colloid Interface Sci. 1968;26:62-9.
[29] Yu J, Duan J, Peng W, Wang L, Peng P, Jiang P. Influence of nano-AlN particles on thermal conductivity, thermal stability and cure behavior of cycloaliphatic epoxy/trimethacrylate system. Express Polym. Lett. 2011;5:132-41.
[30] Zabihi O, Khayyam H, Fox BL, Naebe M. Enhanced thermal stability and lifetime of epoxy nanocomposites using covalently functionalized clay: experimental and modelling. New J. Chem. 2015;39:2269-78.
[31] Bhowmick DK, Linden S, Devaux A, De Cola L, Zacharias H. Functionalization of amorphous SiO_2 and 6H-SiC(0001) surfaces with benzo[ghi]perylene-1,2-dicarboxylic anhydride via an APTES linker. Small 2012;8:592-601.
[32] Neergaard Waltenburg H, Yates J. Surface chemistry of silicon. Chem. Rev. 1995;95:1589-73.

[33] Zhang D, Karki AB, Rutman D,Young DP, Wang A, Cocke D, et.al. Electrospun polyacrylonitrile nanocomposite fibers reinforced with Fe_3O_4 nanoparticles: fabrication and property analysis. Polymer 2009;50:4189-98.
[34] Yang L, Phua SL, Teo JK, Toh CL, Lau SK, Ma J, et.al. A biomimetic approach to enhancing interfacial interactions: polydopamine-coated clay as reinforcement for epoxy resin. ACS Appl. Mater. Interfaces 2011;3:3026-32.
[35] Cassagnau P. Melt Rheology of organoclay and fumed silica nanocomposites. Polymer 2008;49:2183-96.
[36] Zhu J, Wei S, Ryu J, Sun L, Luo Z, Guo Z. Magnetic epoxy resin nanocomposites reinforced with core−shell structured Fe@FeO nanoparticles: fabrication and property analysis. ACS Appl. Mater. Interfaces 2010;2:2100-7.
[37] Lee JH, Um CM, Lee Ib. Rheological properties of resin composites according to variations in monomer and filler composition. Dent. Mater. 2006;22:515-26.
[38] Gu H, Guo J, Wei H, Yan X, Ding D, Zhang X, et.al. Transparent anhydride–cured epoxy nanocomposites reinforced with polyaniline stabilized nanosilica. J. Mater. Chem. C 2015;3:8152-65.
[39] Lin Jr C, Hergenrother WL, Hilton AS. Mooney viscosity stability and polymer filler interactions in silica filled rubbers. Rubber Chem. Technol. 2002;75:215-45.
[40] Gu H, Tadakamalla S, Huang Y, Colorado HA, Luo Z, Haldolaarachchige, N, et.al. Polyaniline stabilized magnetite nanoparticle reinforced epoxy nanocomposites. ACS Appl. Mater. Interfaces 2012;4:5613-24.
[41] Gu H, Tadakamalla S, Zhang X, Huang Y, Jiang Y, Colorado H, et.al. Epoxy resin nanosuspensions and reinforced nanocomposites from polyaniline stabilized multi-walled carbon nanotubes. J. Mater. Chem. C 2013;1:729-43.
[42] Nouri N, Ziaei-Rad S. A molecular dynamics investigation on mechanical properties of cross-linked polymer networks. Macromolecules 2011;44:5481-9.
[43] Gao J, Li J, Benicewicz BC, Zhao S, Hillborg H, Schadler, LS. The mechanical properties of epoxy composites filled with rubbery copolymer grafted SiO_2. Polymers 2012;4;187-210.
[44] Yu W, Fu J, Dong X, Chen L, Jia H, Shi L. Highly populated and nearly monodispersed nanosilica particles in an organic medium and their Epoxy nanocomposites. ACS Appl. Mater. Interfaces 2013;5:8897-906.
[45] Kwon DJ, Wang ZJ, Choi JY, Shin PS, DeVries KL, Park JM. Interfacial and mechanical properties of epoxy composites containing carbon nanotubes grafted with alkyl chains of different length. Compos. Part A: Appl. Sci. Manuf. 2016;82:190-7.
[46] Kim SW, Kim T, Kim YS, Choi HS, Lim HJ, Yang SJ, Park CR. Surface modifications for the effective dispersion of carbon nanotubes in solvents and polymers. Carbon 2012;50:3-33.
[47] Gu H, Guo J, He Q, Tadakamalla S, Zhang X, Yan X, et.al. Flame-retardant epoxy resin nanocomposites reinforced with polyaniline-stabilized silica nanoparticles. Ind. Eng. Chem. Res. 2013;52:7718-28.
[48] Sun YY, Zhang ZQ, Moon KS, Wong CP. Glass transition and relaxation behavior of epoxy nanocomposites. J. Polym. Sci. Pt. B-Polym. Phys. 2004;42:3849-58.
[49] Tarrio-Saavedra J. Controversial Effects of fumed silica on the curing and thermomechanical properties of epoxy composites. Express Polym. Lett. 2010;4:382-95.
[50] Preghenella M, Pegoretti A, Migliaresi C. Thermo-mechanical characterization of

fumed silica-epoxy nanocomposites. Polymer 2005;46:12065-72.
[51] Becker O, Varley R, Simon G. Morphology, thermal relaxations and mechanical properties of layered silicate nanocomposites based upon high-functionality epoxy resins. Polymer 2002;43:4365-73.
[52] Sajjad M, Feichtenschlager B, Pabisch S, Svehla J, Koch T, Seidler S et.al. Study of the effect of the concentration, size and surface chemistry of zirconia and silica nanoparticle fillers within an epoxy resin on the bulk properties of the resulting nanocomposites. Polym. Int. 2012;61:274-85.
[53] Koo B, Liu Y, Zou J, Chattopadhyay A, Dai LL. Study of glass transition temperature (T_g) of novel stress-sensitive composites using molecular dynamic simulation. Model. Simul. Mater. Sci. Eng. 2014;22:1-13.
[54] Liu Y, Zhao J, Zhao L, Li W, Zhang H, Yu X, et.al. High performance shape memory epoxy/carbon nanotube nanocomposites. ACS Appl. Mater. Interfaces 2016;8:311-20.
[55] Dittanet P, Pearson RA. Effect of silica nanoparticle size on toughening mechanisms of filled epoxy. Polymer 2012;53:1890-905.
[56] Suzuki N, Kiba S, Kamachi Y, Miyamoto N, Yamauchi Y. Mesoporous silica as smart inorganic filler: preparation of robust silicone rubber with low thermal expansion roperty. J. Mater. Chem. 2011;21:5338-44.
[57] Teh P, Jaafar M, Akil H, Seetharamu K, Wagiman A, Beh K. Thermal and mechanical properties of particulate fillers filled epoxy composites for electronic packaging application. Polym. Adv. Technol. 2008;19:308-15.
[58] Lin W, Moon KS, Wong CP. A combined process of in situ functionalization and microwave treatment to achieve ultrasmall thermal expansion of aligned carbon nanotube–polymer nnanocomposites: toward applications as thermal interface materials. Adv. Mater. 2009;21:2421-4.
[59] Grassie N, Guy MI, Tennent NH. Degradationof epoxy polymers: part 4-thermal degradation of bisphenol-A diglycidyl ether cured with ethylene diamine. Polym. Degrad. Stabil. 1986;14:125-37.
[60] Zhu J, Wei S, Ryu J, Budhathoki M, Liang G, Guo Z. In situ stabilized carbon nanofiber (CNF) reinforced epoxy nanocomposites. J. Mater. Chem. 2010;20:4937-48.
[61] Zabihi O, Khayyam H, Fox BL, Naebe M. Enhanced thermal stability and lifetime of epoxy nanocomposites using covalently functionalized clay: experimental and modelling. New J. Chem. 2015;39:2269-78.

Scheme captions

Scheme 1. Schematic illustration of (a) Cross-linking mechanism of DGEBF with DETDA curing agent; (b, c) Proposed mechanisms for the reactions between epoxy and amino functional groups in the presence of SNP-NH_2 and SNP-EP.

Scheme 2. Schematic illustration of the interfacial interactions of the (a) SNP, (b) SNP-NH_2, (c) SNP-EP, and (d) SNP-C with the amine cured epoxy system.

Figure captions

Fig. 1. (a) FT-IR spectra and (b) XPS survey spectra of SNP, SNP-NH_2, SNP-EP, SNP-C; (c) N1s XPS spectrum of SNP-NH_2; C1s XPS spectrum of (d) SNP-EP and (e) SNP-C; (f) TGA curves of SNP, SNP-NH_2, SNP-EP, and SNP-C.

Fig. 2. The shear response behaviors of the neat EP and its nanosuspensions with 10 wt% SNP, SNP-NH_2, SNP-EP, and SNP-C under room temperature at (a) 0 h, (b) 24 h, and (c) 48 h; (d) the viscosity of the neat EP and its nanosuspensions at the shear rate of 1 s^{-1} at 0 h, 24 h, and 48 h under room temperature, and inset is the comparison of the viscosity value of the samples after 48 h.

Fig. 3. SEM images of the fractured morphology of (a, b) 10 wt% SNP/epoxy, (c, d) 10 wt% SNP-NH_2/epoxy, (e, f) 10 wt% SNP-EP/epoxy and (g, h) 10 wt% SNP-C/epoxy composites.

Fig. 4. (a) Storage modulus and (c) tan δ as a function of temperature for the cured neat EP and its nanocomposites filled with SNP, SNP-NH_2, SNP-EP, and SNP-C at 10 wt% loading; (b) their E' values at glassy and rubbery state and (d) their T_g values.

Fig. 5. The thermal expansion behavior of the cured EP and its nanocomposites filled with the SNP, SNP-NH_2, SNP-EP, and SNP-C at 10 wt% loading.

Fig. 6. The TGA curves of the cured EP and its nanocomposites filled with the SNP, SNP-NH_2, SNP-EP, and SNP-C at 10 wt% loading.

Tables

Table 1 Thermal properties of the cured neat EP and its nanocomposites

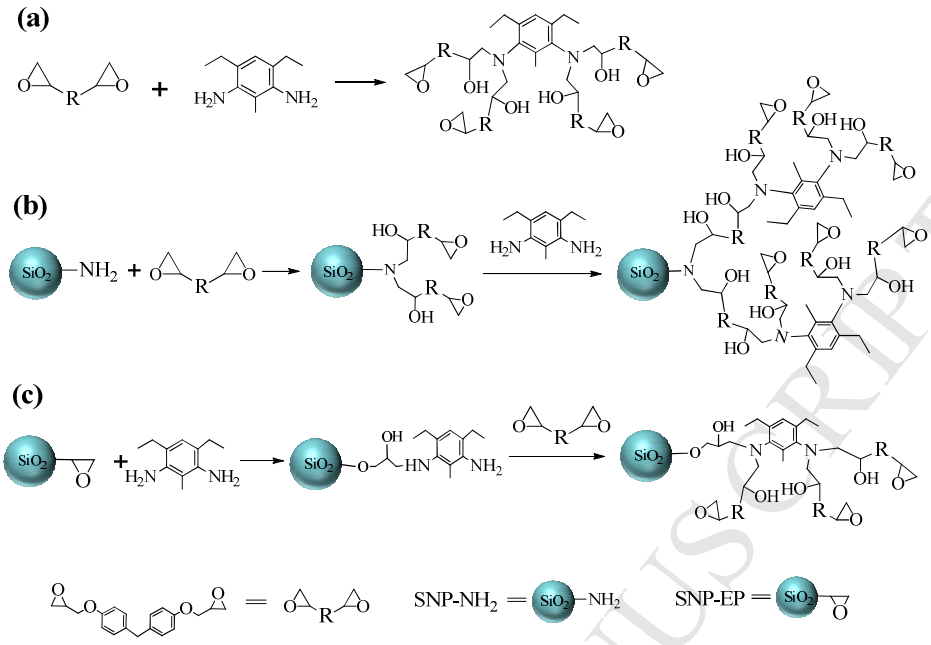

Scheme 1. Schematic illustration of (a) Cross-linking mechanism of DGEBF with DETDA curing agent; (b, c) Proposed mechanisms for the reactions between epoxy and amino functional groups in the presence of SNP-NH_2 and SNP-EP.

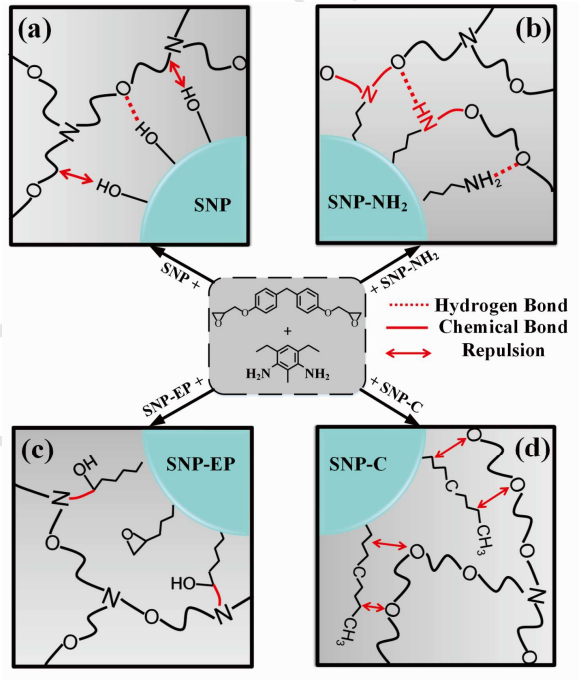

Scheme 2. Schematic illustration of the interfacial interactions of the (a) SNP, (b) SNP-NH_2, (c) SNP-EP, and (d) SNP-C with the amine cured epoxy system.

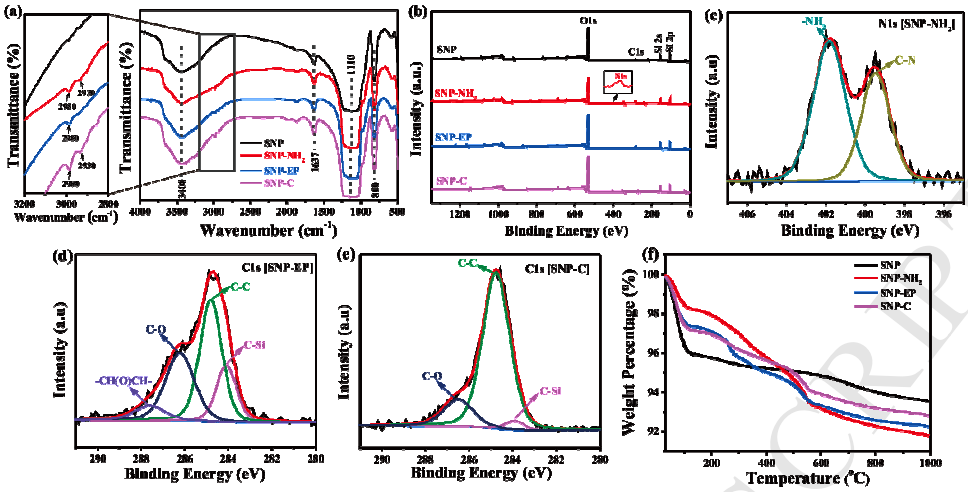

Fig. 1. (a) FT-IR spectra and (b) XPS survey spectra of SNP, SNP-NH_2, SNP-EP, SNP-C; (c) N1s XPS spectrum of SNP-NH_2; C1s XPS spectrum of (d) SNP-EP and (e) SNP-C; (f) TGA curves of SNP, SNP-NH_2, SNP-EP, and SNP-C.

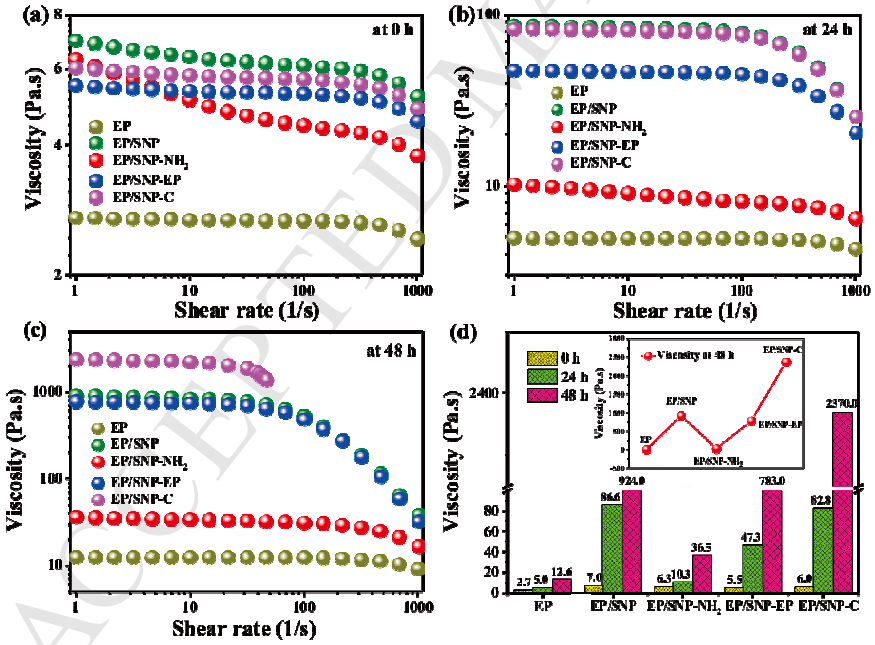

Fig. 2. The shear response behaviors of the neat EP and its nanosuspensions with 10 wt% SNP, SNP-NH_2, SNP-EP, and SNP-C under room temperature at (a) 0 h, (b) 24 h, and (c) 48 h; (d) the viscosity of the neat EP and its nanosuspensions at the shear rate of 1 s^{-1} at 0 h, 24 h, and 48 h under room temperature, and inset is the comparison of the viscosity value of the samples after 48 h.

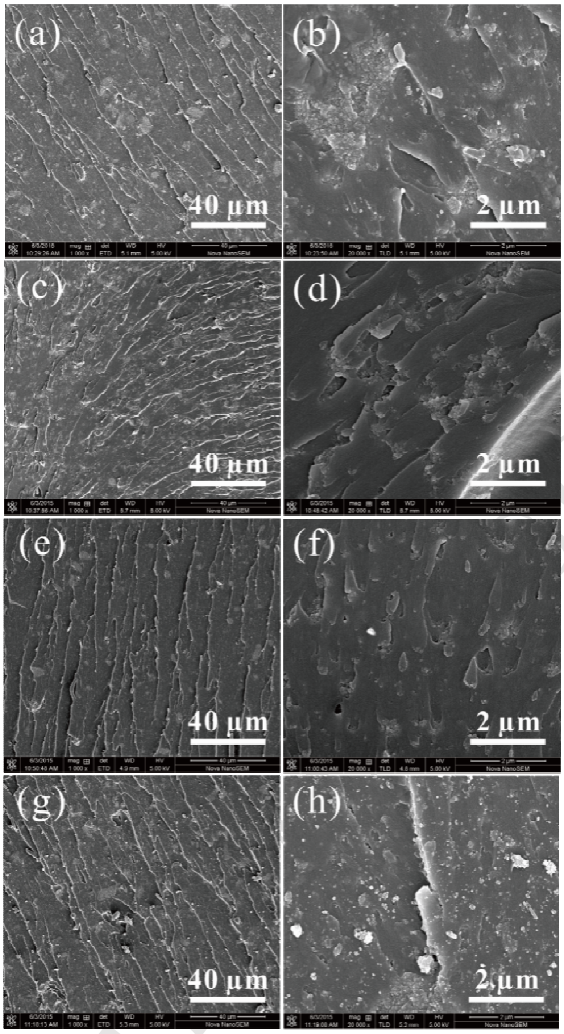

Fig. 3. SEM images of the fractured morphology of (a, b) 10 wt% SNP/epoxy, (c, d) 10 wt% SNP-NH_2/epoxy, (e, f) 10 wt% SNP-EP/epoxy and (g, h) 10 wt% SNP-C/epoxy composites.

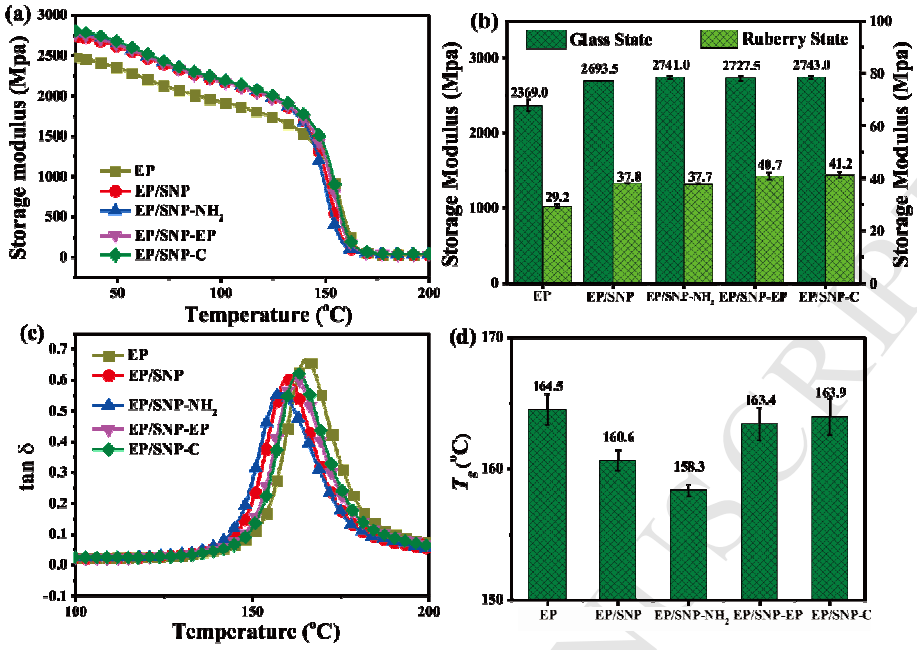

Fig. 4. (a) Storage modulus and (c) tan δ as a function of temperature for the cured neat EP and its nanocomposites filled with SNP, SNP-NH_2, SNP-EP, and SNP-C at 10 wt% loading; (b) their E' values at glassy and rubbery state and (d) their T_g values.

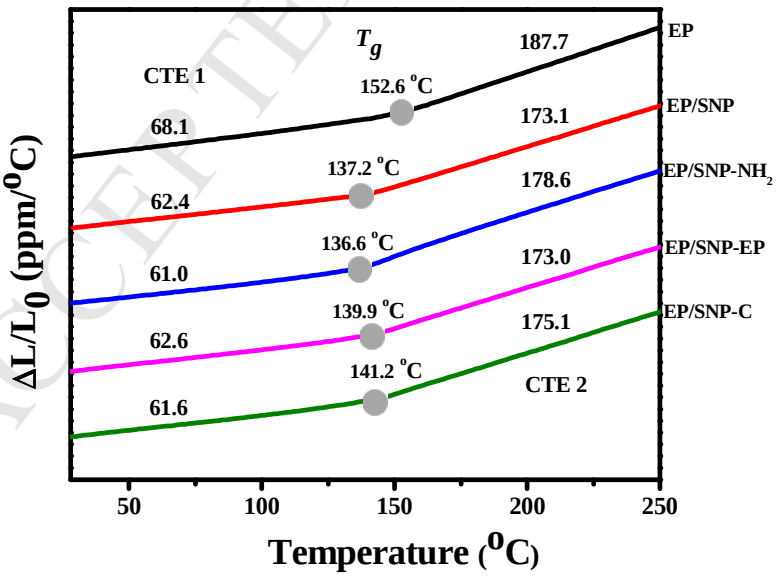

Fig. 5. The thermal expansion behavior of the cured EP and its nanocomposites filled with the SNP, SNP-NH_2, SNP-EP, and SNP-C at 10 wt% loading.

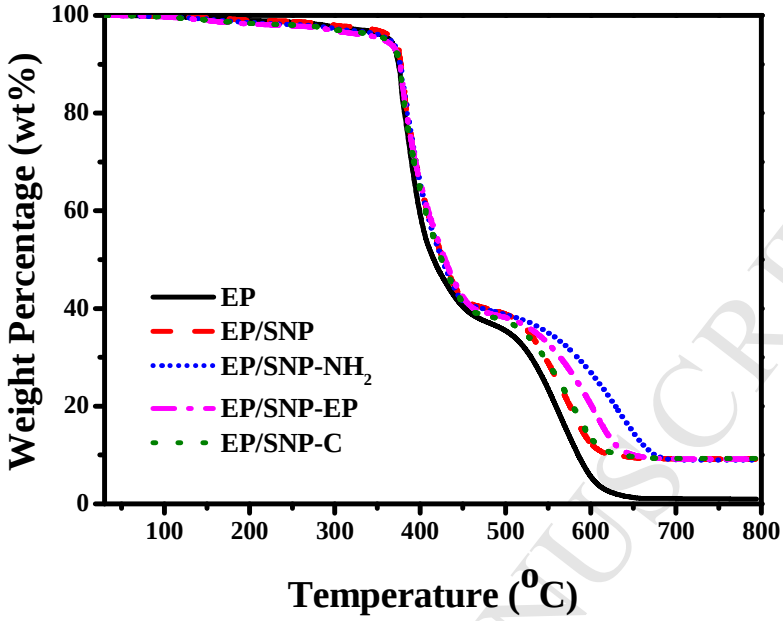

Fig. 6. The TGA curves of the cured EP and its nanocomposites filled with the SNP, SNP-NH_2, SNP-EP, and SNP-C at 10 wt% loading.

Table 1 Thermal properties of the cured neat EP and its nanocomposites

Sample Type	Mean Storage Modulus		Mean T_g		CTE		TGA		
	Glassy State (MPa)	Rubbery State (MPa)	From DMA (°C)	From TMA (°C)	Below T_g (ppm °C^{-1})	Above T_g (ppm °C^{-})	$T_{10\%}$ (°C)	$T_{50\%}$ (°C)	$T_{70\%}$ (°C)
EP	2369.0	29.2	164.5	152.6	68.1	187.7	374.6	416.0	530.0
EP/SNP	2693.5	37.8	160.6	137.2	62.4	173.1	377.6	426.8	546.3
EP/SNP-NH_2	2741.0	37.7	158.3	136.6	61.0	178.6	376.1	425.5	583.9
EP/SNP-EP	2727.5	40.7	163.4	139.9	62.6	173.0	375.8	428.9	563.9
EP/SNP-C	2743.0	41.2	163.9	141.2	61.6	175.1	375.6	425.0	545.4